Phase formation sequence in the Ti/InP system during thin film solid-state reactions

E. Ghegin, Ph. Rodriguez, J. L. Lábár, M. Menyhárd, S. Favier, I. Sagnes, and F. Nemouchi

Citation: Journal of Applied Physics **121**, 245311 (2017); doi: 10.1063/1.4990427
View online: http://dx.doi.org/10.1063/1.4990427
View Table of Contents: http://aip.scitation.org/toc/jap/121/24
Published by the American Institute of Physics

Articles you may be interested in

Oxidation kinetics of Si and SiGe by dry rapid thermal oxidation, in-situ steam generation oxidation and dry furnace oxidation
Journal of Applied Physics **121**, 245308 (2017); 10.1063/1.4987040

Twin domains in epitaxial thin MnSi layers on Si(111)
Journal of Applied Physics **121**, 245310 (2017); 10.1063/1.4990284

Magnetic domain walls in nanostrips of single-crystalline Fe_4N(001) thin films with fourfold in-plane magnetic anisotropy
Journal of Applied Physics **121**, 243904 (2017); 10.1063/1.4989991

Excitonic complexes in strain-free and highly symmetric GaAs quantum dots fabricated by filling of self-assembled nanoholes
Journal of Applied Physics **121**, 245702 (2017); 10.1063/1.4989808

Noise, gain, and capture probability of p-type InAs-GaAs quantum-dot and quantum dot-in-well infrared photodetectors
Journal of Applied Physics **121**, 244501 (2017); 10.1063/1.4989834

Influence of ion implantation parameters on the perpendicular magnetic anisotropy of Fe-N thin films with stripe domains
Journal of Applied Physics **121**, 243903 (2017); 10.1063/1.4986653

AIP | Journal of Applied Physics
Save your money for your research.
It's now FREE to publish with us -
no page, color or publication charges apply.
Publish your research in the Journal of Applied Physics to claim your place in applied physics history.

JOURNAL OF APPLIED PHYSICS **121**, 245311 (2017)

Phase formation sequence in the Ti/InP system during thin film solid-state reactions

E. Ghegin,[1,2,3,a)] Ph. Rodriguez,[2] J. L. Lábár,[4] M. Menyhárd,[4] S. Favier,[1,2] I. Sagnes,[5] and F. Nemouchi[2]
[1]*STMicroelectronics, 850 rue Jean Monnet, BP 16, 38926 Crolles, France*
[2]*Univ. Grenoble Alpes, F-38000 Grenoble, France and CEA, LETI, MINATEC Campus, F-38054 Grenoble, France*
[3]*CNRS-C2N, Route de Nozay, 91460 Marcoussis, France*
[4]*MTA EK MFA, Konkoly Thege M. u. 29-33, H-1121 Budapest, Hungary*
[5]*Centre de Nanosciences et de Nanotechnologies, CNRS, Univ. Paris-Sud, Université Paris-Saclay, C2N-Marcoussis, 91460 Marcoussis, France*

(Received 14 March 2017; accepted 14 June 2017; published online 30 June 2017)

The metallurgical properties of the Ti/InP system meet a great interest for its use as a contact in the scope of various applications such as the Si Photonics. The investigations conducted on this system highlight the initiation of a reaction between the Ti and the InP substrate during the deposition process conducted at 100 °C. The simultaneous formation of two binary phases, namely, Ti_2In_5 and TiP, is attributed to the compositional gradient induced in the InP by the wet surface preparation and enhanced by the subsequent *in situ* Ar^+ preclean. Once formed, the TiP layer acts as a diffusion barrier inhibiting further reaction up to 450 °C in spite of the presence of an important Ti reservoir. At higher temperature, however, i.e., from 550 °C, the reaction is enabled either by the enhancement of the species diffusion through the TiP layer or by its agglomeration. This reaction gives rise to the total consumption of the Ti_2In_5 and Ti while the TiP and In phases are promoted. *Published by AIP Publishing.* [http://dx.doi.org/10.1063/1.4990427]

I. INTRODUCTION

Allowing data rates beyond what electronic components can offer, photonics have been identified as one promising paradigm. However, while silicon is of huge interest for the making of most components, its indirect band gap prevents it from being an efficient light emitter. For addressing this issue, III-V semiconductor compounds have been introduced as potential candidates. Among them, n-InP substrates and the corresponding metal interfaces have been extensively studied for improving the performances of such devices. Among others, Ti is one of the most widely used metals in the classical Ti/Pt/Au contacts, where it provides the primary role of improved metallization adhesion.[1] In these stacks, the Ti being directly in contact with the semiconductor mainly rules the electrical properties of the integrated contacts. Therefore, in the scope of forming noble material-free contacts, the study of alloyed Ti-based metallizations is of particular interest.

In order to make such contacts, the main process flow consists of a surface preparation (wet and/or plasma treatments), one or several metal layer depositions and a heat treatment. These processes aim to control the intermetallic compound(s) formation, thereby modifying the contact resistivity. Each phase arising from the solid state reactions offers various electrical properties (resistivity, work function, Schottky barrier height, interface and gap defects…) and thermokinetic properties (dopant and/or element distribution, growth kinetics, thermal stability, texture…). As a consequence, it is necessary to identify the phase formation sequence along with the range of existence of each compound.

Most studies present in the literature report the initiation of a reaction between the Ti and the InP during the deposition process, without any critical minimum coverage.[2–6] Some In release is featured and associated with the formation of intermixed Ti-P layer;[2–6] only one study does not report the formation of intermixed compound during the deposition process but identifies the first signs of reaction at 325 °C.[7] At higher temperatures, however, i.e., from 300 °C to 350 °C depending on the studies, all authors found out that the intermixed layer is converted into stable crystalline binary Ti-P intermetallic compounds. The composition of the latter is not ascertained but might comprise some TiP and/or Ti_4P_3. However, even if both phases coexist, the TiP appears to be predominant. The formation of these compounds is associated with some In out diffusion and with an incomplete consumption of the Ti. As a consequence, the authors conclude that the TiP phase acts as a diffusion barrier thereby inhibiting further reaction between the Ti and the InP even at temperatures as high as 600 °C.

In this paper, we investigate the phase sequence obtained on the Ti (20 nm or 50 nm)/InP systems under rapid thermal processes (RTP) and identify the mechanisms responsible for the appearance of the various observed phases.

II. EXPERIMENTAL PROCEDURE

The metallurgical studies were carried out on semi-insulating (001) InP substrates on top of which a 300 nm InP

[a)]Author to whom correspondence should be addressed: elodie.ghegin@st.com

epitaxial layer was grown. The substrate cleaning procedure includes a 30 s wet etching in dilute HCl:H_2O (1:2) solution followed by a direct Ar^+ plasma etching (RF1: 130 W; RF2: 310 W) prior to the metal deposition process. The 20 and 50 nm-thick titanium films were deposited by physical vapor deposition (magnetron sputtering in DC mode) at 100 °C and capped by 7 nm thick TiN films deposited at the same temperature. This kind of encapsulation protects the Ti film from any atmospheric contamination and/or oxidation, which could alter the reactions taking place at the Ti/InP interface. The Ar^+ preclean and the deposition of the metal layers were performed in the same equipment, thereby avoiding air breaks. Then, RTP processes were conducted under NH_2 ambient for 60 s at temperatures ranging from 250 °C to 550 °C.

Both, the as deposited and the reacted films were characterized by Auger Electron Spectroscopy (AES) and cross sectional Transmission Electron Microscopy (TEM). Samples dedicated to the TEM analysis were prepared by focused Ga^+-ion beam (FIB) and Ar^+-ion milling. All samples were also characterized thanks to X-Ray Diffraction (XRD) detexturation. Detexturation consists in acquiring $\theta/2\theta$ diffractograms at several χ angles (8 scans from 0 to 70° by steps of 10°—see Appendix A for the description of the various angles of a four-circle diffractometer). The sum of all these diffractograms gives access to a higher number of diffraction lines, as well as higher peak intensity. This kind of XRD is well optimized for thin films because they are often textured, and their diffracting volume is small, especially, in the early stages of their formation.

III. RESULTS

A. As deposited systems

The Ti being known as a very reactive metal on InP, the composition of the Ti/InP system right after deposition was determined thanks to the XRD detexturation. For doing so, several Ti thicknesses ranging from 20 to 50 nm were probed as displayed in Fig. 1.

In accordance with most results reported in literature, the XRD patterns highlight the initiation of the reaction between Ti and InP during the deposition process.[2–6] This reaction appears to be incomplete as several peaks corresponding to the Ti are still observed, even when only 20 nm of metal were initially deposited. The XRD patterns highlight the formation of at least two binary and crystalline phases, the hexagonal TiP, and the tetragonal Ti_2In_5. While the formation of the first phase is largely reported in literature, the second has not been observed yet. It is important to note that some In might also be present in these systems as one peak might be attributed to this phase ($2\theta = 33°$). However, this assumption could hardly be affirmed, thanks solely to the XRD, as this peak could also be attributed to TiP. Therefore, in order to identify more precisely the nature and the repartition of the various phases, additional TEM combined with AES characterizations were conducted on the TiN (7 nm)/Ti (20 nm)/InP and TiN (7 nm)/Ti(50 nm)/InP systems (Figs. 2 and 3).

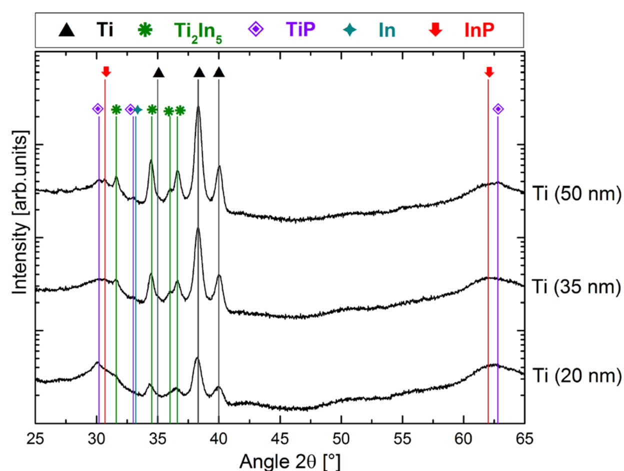

FIG. 1. XRD detexturation patterns of the as deposited TiN (7 nm)/Ti (20, 35, and 50 nm)/InP samples.

The low magnification TEM images highlight the homogeneity and the continuity of the layers present on the InP [Fig. 2(a)]. Increasing the magnification reveals the presence of two different layers underneath the Ti whose grains are about 40 nm wide [Fig. 2(b)]. Although both layers' thicknesses are not perfectly homogeneous within each system, they are independent of the initially deposited Ti thickness:

- The thickness of layer-1 ranges from 3 nm to 8 nm within each sample;
- The thickness of layer-2 ranges from 7 nm to 15 nm within each sample.

Selected Area Electron Diffraction (SAED) pattern and its indexation are shown in Fig. 2(c). When a diffraction spot can be attributed to more than one phase, the most probable is given in first. Even if SAED technique does not probe the same interreticular planes than XRD, it exhibits the presence of the same phases Ti, TiN, TiP, and Ti_2In_5. Additionally, the TEM cross section features an important contrast in terms of composition between the two layers. Taking into account the atomic masses of Ti (47.87 g mol^{-1}), In (114.82 g mol^{-1}), and P (30.97 g mol^{-1}), and the results obtained on the XRD characterization, one must reasonably assume that the observed stack is composed of TiN/Ti/Ti_2In_5/TiP/InP. Additional AES characterizations were conducted in order to confirm or deny this conclusion. Because they are very similar, Fig. 3 displays solely the results corresponding to the system TiN (7 nm)/Ti (20 nm)/InP.

As supported by the AES depth profile, the two layers present very different compositions. The AES depth profiles are smeared due to the roughness of the corresponding layers. While the layer in contact with the Ti (layer-2) is composed of a mixture of Ti and In, the layer in contact with the InP (layer-1) consists of Ti and P. As a consequence, the various characterizations indicate the fact that the Ti reacts with the InP during the deposition process conducted at 100 °C to form the layered structure: TiN (7 nm)/Ti/Ti_2In_5 (7 to 15 nm)/TiP (3 to 8 nm)/InP.

B. Annealed samples

In order to determine the evolution of the structure identified after deposition, additional characterizations were

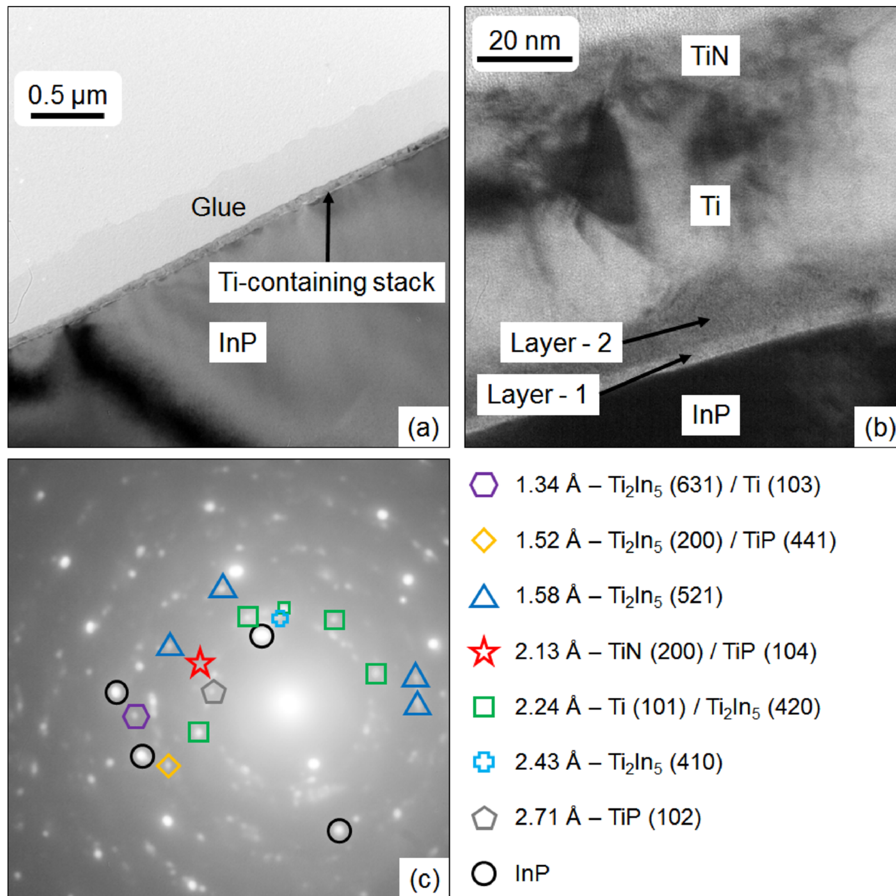

FIG. 2. Bright field TEM cross section of (a) the TiN (7 nm)/Ti (20 nm)/InP as deposited sample in low magnification, (b) the TiN (7 nm)/Ti (50 nm)/InP as deposited sample in high magnification and (c) the corresponding SAED pattern highlighting the presence of four different layers in the system.

conducted on samples annealed thanks to RTP processes at temperatures ranging from 250 to 550 °C. The XRD detexturation patterns corresponding to these samples are presented in Figs. 4 and 5, for initial Ti thicknesses of 20 and 50 nm, respectively.

When only 20 nm of Ti are initially deposited, the diffractograms highlight the coexistence of the three phases already observed, i.e., Ti, Ti_2In_5, and TiP, at temperatures up to 450 °C (Fig. 4). Furthermore, the intensity of every diffraction peak is constant throughout the annealing temperatures, and thus, do not indicate the evolution of the phases from 250 to 450 °C. However, increase in the initial Ti thickness to 50 nm leads to a modification of the behavior of the diffraction peak (Fig. 5). Indeed, peaks corresponding to the Ti_2In_5 and the TiP are not present in all the samples, and most importantly, seem to disappear at some temperature. For example, one of the most intense TiP peak ($2\theta = 30.3°$) is absent at 250 °C, while the XRD analyses conducted after deposition and at higher temperatures indicate the presence of this compound in the corresponding systems. Similarly, all the peaks corresponding to the Ti_2In_5 at angles ranging

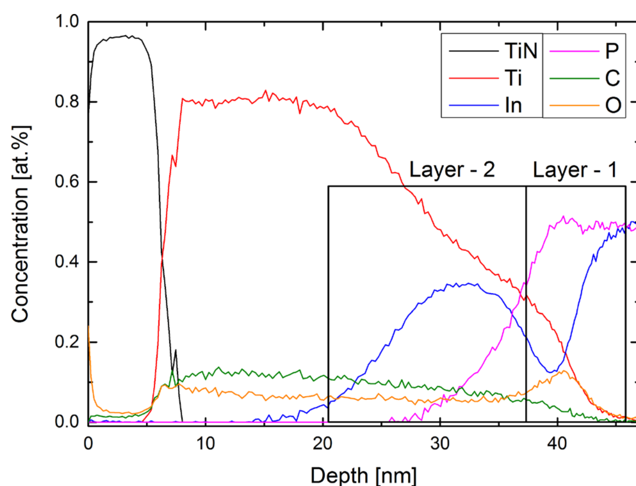

FIG. 3. AES depth profile corresponding to the as deposited TiN (7 nm)/Ti (20 nm)/InP system.

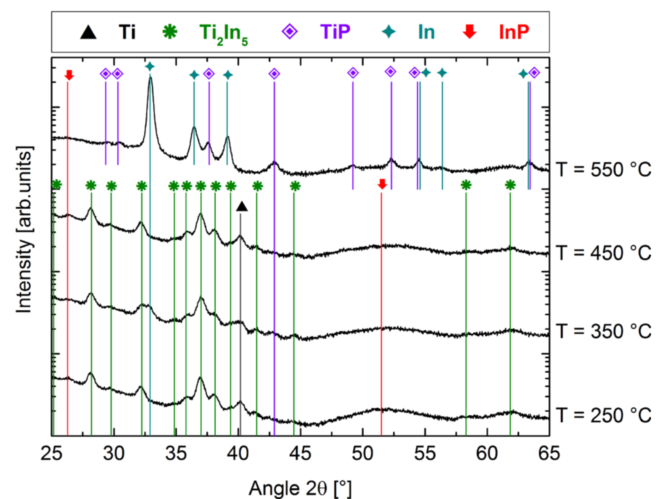

FIG. 4. XRD detexturation patterns of the TiN (7 nm)/Ti (20 nm)/InP samples annealed at 250, 350, 450, and 550 °C for 60 s (RTP). A 2° offset on the incident beam was applied in order to minimize the InP substrate contribution.

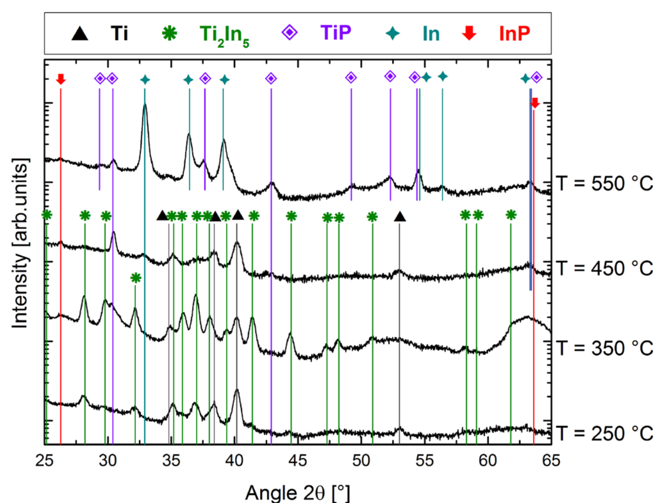

FIG. 5. XRD detexturation patterns of the TiN (7 nm)/Ti (50 nm)/InP samples annealed at 250, 350, 450, and 550 °C for 60 s (RTP). A 2° offset on the incident beam was applied in order to minimize the InP substrate contribution.

from 45° to 65° are absent in the patterns acquired after annealing treatments conducted at 250 °C and 450 °C while they are present at 350 °C. Therefore, the extinction of some peaks seems to be uncorrelated with the actual composition of the systems and may be attributed to the combined effect of the measurement geometry and the crystallographic texture of these compounds. Indeed, even though diffractograms were acquired at several χ angles to give rise to the summed patterns presented in Figs. 4 and 5, no rotation was performed around the ϕ angle in this configuration (A schematic representation of the different angles of a four-circle diffractometer is shown in Fig. 11 in Appendix A). Therefore, some orientations might be extinct depending on the initial positioning of the sample/wafer with respect to the X-Ray beam. In order to confirm or deny this hypothesis, TEM and AES characterizations were conducted on the system presenting an initial Ti thickness of 50 nm annealed at 450 °C (Fig. 6).

The TEM cross section along with the AES depth profile feature the presence of four distinct layers, which are very similar to the ones observed after deposition in terms of morphology and thicknesses. The layer 1 in contact with the InP substrate and composed of Ti and P is still about 3–8 nm thick, while the thickness of the layer 2 composed of Ti and In, still ranges from 7 to 15 nm. Note that the roughness present in this system results in transitions that are less net on the corresponding AES depth profile. As a consequence, the layer's thicknesses are somewhat overestimated in this profile compared to the ones actually measured in the corresponding TEM cross sections and presented here. However, although the roughness seems to be increased by this thermal treatment, the various compounds are still arranged in the layered structure already observed after deposition: TiN (7 nm)/Ti/Ti_2In_5 (7 to 15 nm)/TiP (3 to 8 nm)/InP. As a consequence, the modification of the diffractograms from 250 °C to 450 °C is most likely linked to a texture of the observed compounds rather than to an actual modification of the systems' composition. For initially deposited Ti thickness ranging from 20 to 50 nm, the TiP and the Ti_2In_5 are formed during the

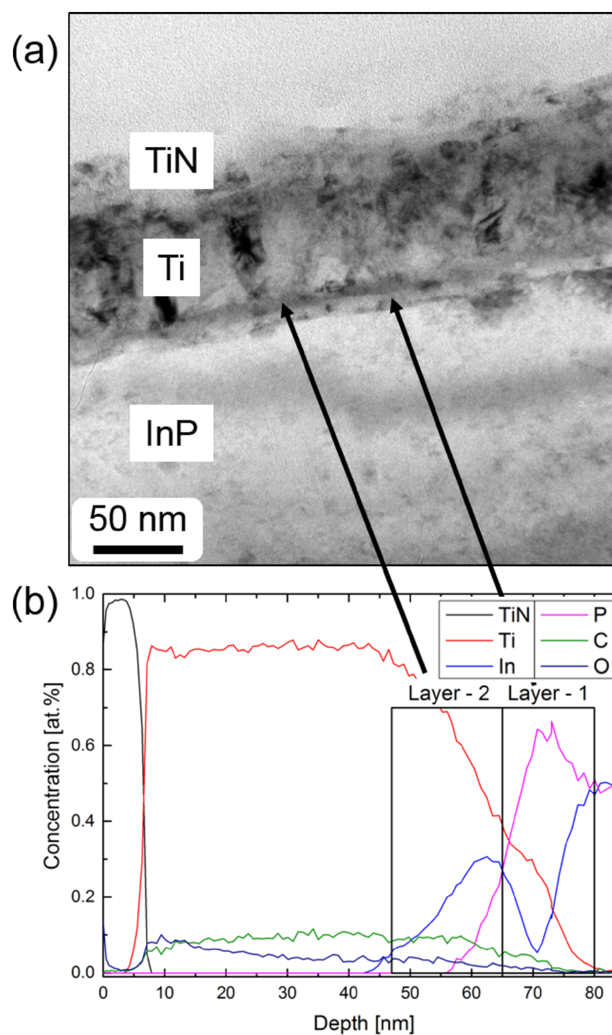

FIG. 6. (a) TEM cross section of the TiN (7 nm)/Ti (50 nm)/InP system annealed at 450 °C and (b) corresponding AES depth profile.

deposition process and are stable in terms of composition and thicknesses at temperatures as high as 450 °C.

However, contrary to the observations made in this range of temperature, a drastic change of composition is brought by an increase in the temperature to 550 °C. At this point, a complete redistribution of the species present in the sample leads to the total consumption of the Ti and Ti_2In_5. The latter are replaced by the already observed TiP phase. The stoichiometry conservation leads to some In release as confirmed by the corresponding XRD patterns.

IV. DISCUSSION

In Sec. III, thanks to the combined results emanating from XRD, TEM, and AES, the composition of Ti (20 to 50 nm)/InP systems was determined from deposition temperature to 550 °C. It was found that a layered structure composed of Ti, Ti_2In_5 and TiP is formed during the deposition process conducted at 100 °C and is stable up to 450 °C. However, further increasing the temperature up to 550 °C leads to a consumption of the Ti and the Ti_2In_5 to promote the TiP and In.

The initial appearance of Ti-In phases along with Ti-P phases has not been reported yet in this kind of systems.

Because it might modify their electrical properties or their thermal stability, the phenomena responsible for the appearance of the Ti_2In_5 are worth identifying. Similar discrepancies were observed on other systems and attributed to the different data treatment used by the various groups.[8,9] In our case, the identification of the phases could hardly be questioned as a multitude of diffracting peaks confirms the indexation of each phase in Figs. 4 and 5. However, as detailed in the experimental procedure, all samples were dipped into a concentrated HCl solution and subjected to an Ar^+ preclean before the metallization deposition in order to remove the native oxides and contaminants from the InP surface. Studies concerning the effect of these surface preparations showed that both treatments modify the InP surface's stoichiometry.[10–14]

A. Impact of the InP surface preparation

In order to further understand the individual effect of the wet and the dry preparation on our systems, two additional samples were prepared. The first one was only dipped in the HCl: $H_2O = (1: 2)$ wet solution while the second one was additionally submitted to the Ar^+ plasma. In order to avoid Ti and InP intermixing, no Ti layer was deposited. However, the 7 nm-thick TiN layer was deposited on the InP immediately after the surface preparations in order to prevent any parasitic oxidation or contamination of its surface. The TEM images along with the corresponding AES depth profiles are presented in Fig. 7.

The TEM image corresponding to the sample that was subjected to the Ar preclean [Fig. 7(a)] features an important roughness with a discontinuous TiN film, which morphology is determined by the individual TiN grains. An amorphous layer of about 10 nm is also identified, similarly to the results reported in a previous study.[13] Because of the important roughness, the corresponding AES depth profile is highly smeared and the signals emanating from the InP, the amorphous layer, and the TiN top layer are not clearly distinct. Nonetheless, a compositional gradient can be observed in the profile. It, therefore, appears that this kind of plasma leads to a phosphorus depletion of the InP surface consistently with what was previously reported in the literature.[10–13] The region situated below this In-rich area appears to be P-rich over a few nanometers. One can notice an O signal emanating from the top region of the sample. Because of the important roughness, it would not be possible to assert if it comes from the original InP surface or an oxidation occurring

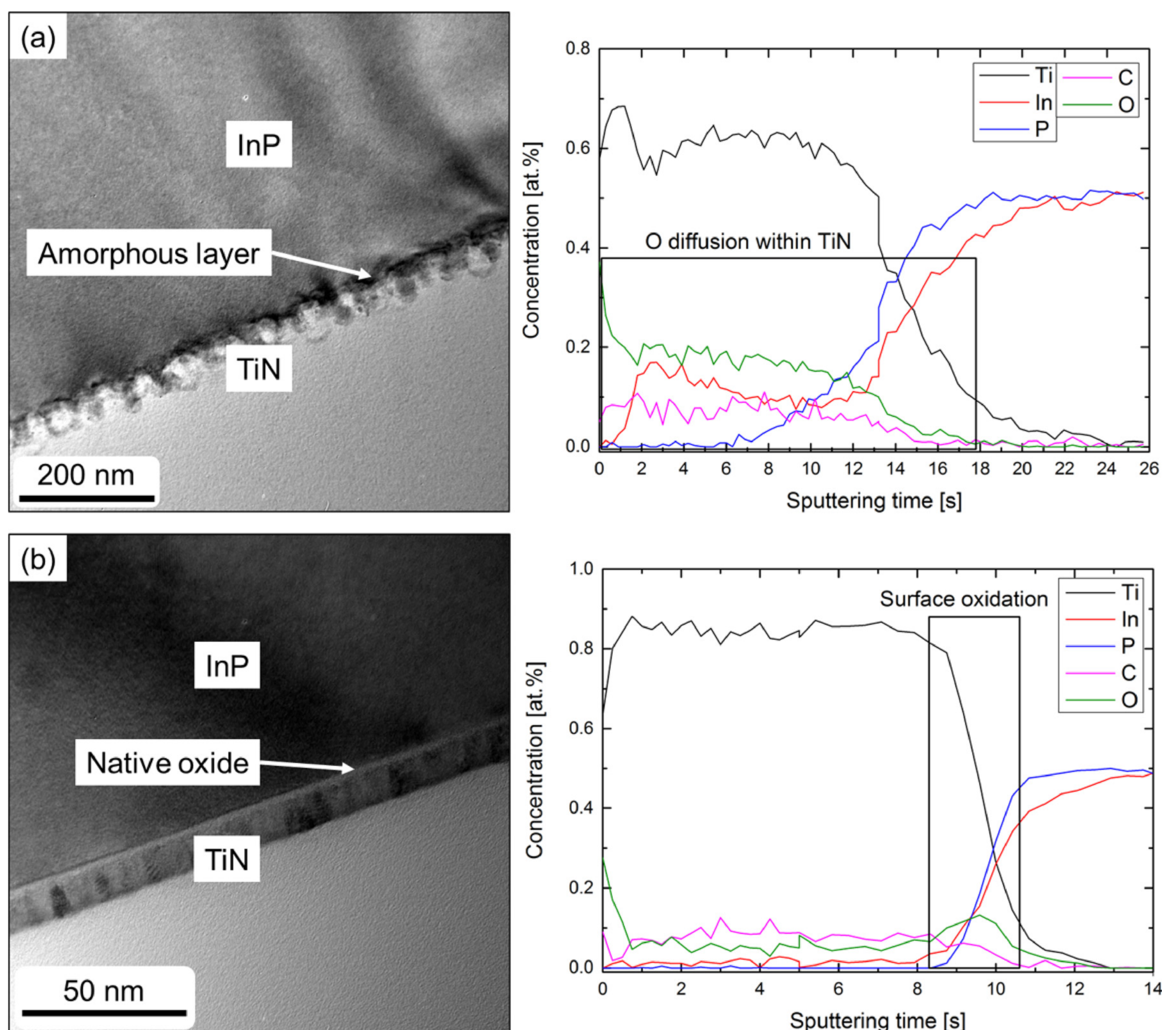

FIG. 7. Bright field TEM images and corresponding AES depth profiles of TiN (7 nm)/InP samples (a) after an HCl: $H_2O = 1: 2$ wet surface preparation combined with an *in situ* Ar^+ plasma treatment and (b) after an HCl: $H_2O = 1: 2$ wet surface preparation.

afterwards because of the TiN layer discontinuity. However, studies conducted in our group showed the efficiency of this kind of InP surface preparation, and are, therefore, in favor of the second hypothesis.[12] When no plasma treatment is conducted, the morphology of the layers drastically changes [Fig. 7(b)]. The TiN layer observed in this case is continuous and homogeneous, which results in a net AES depth profile. In the latter, the various layers can be clearly distinguished from one another. Particularly, the presence of an oxide layer on the InP surface comes as no surprise because of the absence of *in situ* surface preparation before the metal deposition. This native oxide, which is 2 to 3 nm thick can be seen in the corresponding TEM cross section. A compositional gradient similar to the one observed after the Ar^+ plasma treatment is also observed within this native oxide. It, therefore, appears that the wet surface preparation conducted before the *in situ* preclean starts to deplete P from the InP surface. This assumption is in accordance with the findings of Cuypers *et al.* who showed that at high concentrations ($[HCl] \geq 2$ M), the HCl molecule is not dissolved within the solution and anisotropically etches the InP surface.[14] This etching process results in the formation of terraces, which are preferentially In-terminated. Therefore, the creation of a compositional gradient at the surface of the InP is first induced by concentrated HCl solutions and strongly emphasized by the *in situ* Ar^+ plasma treatments.

B. Mechanisms involved in the phase formation sequence

In accordance with literature, our results highlight the fact that both the concentrated HCl solution and the Ar^+ plasma treatment create an amorphous layer, which presents a compositional gradient at the InP surface. The latter is, thus, In-rich at its top and P-rich at its bottom. During the subsequent Ti deposition, which is conducted by PVD at 100 °C, the atoms are deposited on this modified surface. Some atoms are directly in contact with the In-rich region while a non-negligible portion also reaches the P-rich InP area, either thanks to their kinetic energy and/or thanks to a short length diffusion process. The compositional gradient present in the InP, therefore, leads to the formation of two distinct layers, the Ti_2In_5 in the In-rich region and the TiP below. This situation is schematically represented in Fig. 8.

In order to identify more precisely the involved mechanisms, one must additionally consider the results presented in literature. In most studies, no extensive details are given concerning the surface preparation, with the exception of Takeya *et al.* who dipped their InP substrates into HF solutions.[3,4] It is, therefore, consistent to assume that the InP surfaces used in these studies have not been modified, and are thus, composed of 50 at. % of In and 50 at. % of P. As a consequence, it appears that when the InP surface's stoichiometry is not modified, the formation of Ti-P phases is favored at temperatures as low as 20 °C. This observation leads to two conclusions

(i) The gain in free energy (ΔG_v) associated with the formation of TiP in unmodified InP is so important that it compensates the increase of surface energy ($\Delta\sigma$) linked to the nucleation of the phase at temperatures as low as 20 °C. Therefore, the formation of this compound is not limited by the nucleation on intact InP and is thermodynamically favourable on this kind of surface.

(ii) The overall gain in free energy (ΔG_n) associated with the formation of TiP when Ti and unmodified InP are brought in contact is more important than the one associated with the formation of Ti_2In_5. Note that ΔG_n takes into account the gain in free energy associated with the formation of the binary phase (ΔG_v) and the surface energy required for the forming of new interfaces ($\Delta\sigma$).

On the other hand, when the InP surface is modified by the surface preparation and becomes In-rich, these considerations are no longer verified. The kinetic energy due to the PVD deposition brings Ti atoms close to/into the modified layer. In this case, even if the free energy gain would have been maximized by forming the TiP phase, the Ti_2In_5 phase is favored because of the available In excess. Just like TiP, the gain in free energy associated with the formation of Ti_2In_5 compensates the surface energy required for forming the nuclei at temperatures as low as 100 °C. The appearance of this phase is, therefore, not limited by the nucleation process. However, because the TiP phase is thermodynamically more stable in intact InP surfaces, the system tends to form this phase in the regions where the nominal InP stoichiometry is preserved, i.e., below the top few InP nanometers. The formation of Ti-P phases is even more favored in the present case as a P-rich region is present right below the In-rich layer. These mechanisms are in accordance with the

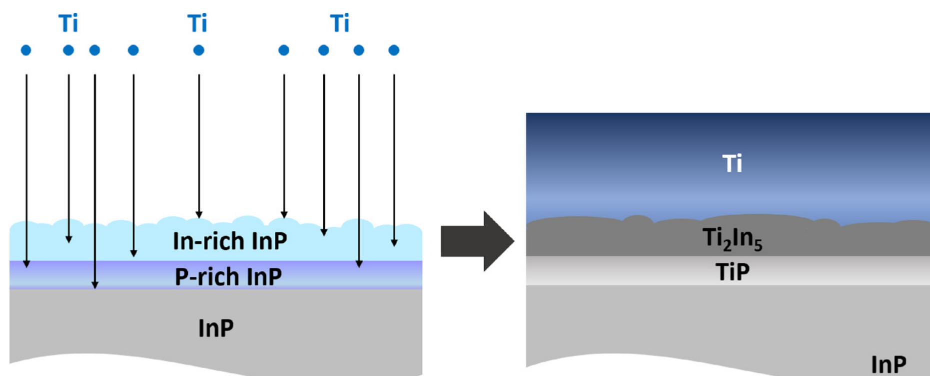

FIG. 8. Schematic representation of the formation of the Ti_2In_5 and TiP phase during the deposition process.

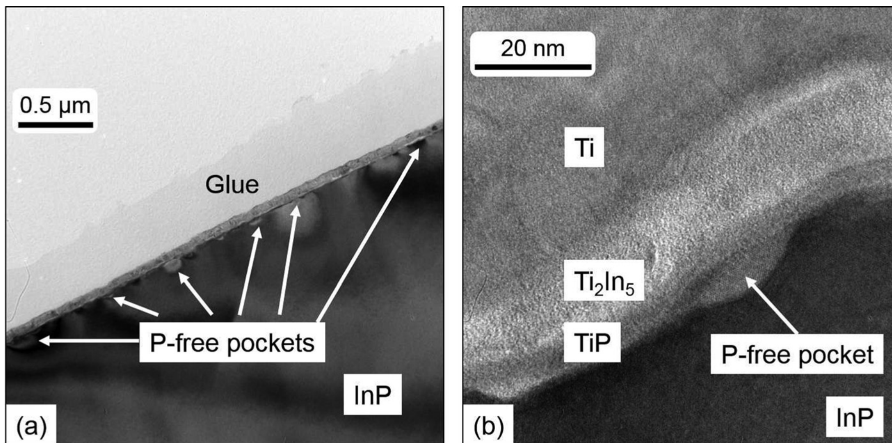

FIG. 9. TEM cross section of the as deposited TiN (7 nm)/Ti (20 nm)/InP system showing the presence of P-free pockets below the TiP layer.

observed layered structure, where the P-rich phase lies below the In-rich one. Furthermore, the formation of the Ti_2In_5 and TiP must occur simultaneously. The P release associated with the appearance of the Ti_2In_5, therefore, helps the formation of the TiP; similarly, the In released during the formation of the TiP is at least partially consumed to form the Ti_2In_5. Once continuous TiP and Ti_2In_5 layers are formed, at least one of them acts as a diffusion barrier (bulk and/or grain boundary diffusion), therefore, inhibiting further reaction up to 450 °C. It is important to note that even though both layers can inhibit the diffusion, based on literature, the TiP probably plays the most important role. Additionally, P-free "pockets" are observed below the TiP layer as displayed in Fig. 9. One can reasonably assume that these pockets appear during the formation of the TiP layer. As mentioned above, when the Ti and the InP react together to form the TiP, some In must be released. A certain proportion of the In participates in the formation of the Ti_2In_5 provided that it is not blocked by the TiP diffusion barrier. However, the proportion of In that is released underneath this TiP layer cannot diffuse through it or in the InP substrate, and is, therefore, constrained to stay in the TiP/InP interface. These pockets are, therefore, composed of pure In whose peaks are observed in the corresponding diffractograms.

As a consequence, it appears that the Ti_2In_5 and the TiP are most probably formed simultaneously during the deposition process by reaction between the Ti and the InP surface submitted by the two steps surface preparation. Once the TiP layer is thick enough to be continuous, the reaction is inhibited, and the system is stable up to 450 °C. At higher temperatures, however, i.e., at 550 °C, a drastic change of composition is observed as the system is only composed of TiP and In. Therefore, during this annealing process, the Ti_2In_5 is decomposed into In, which strongly diffracts into additional Ti. This additional Ti along with the originally deposited one must meet the P contained in the substrate in order to enable the growth of the TiP.

Therefore, a path must be created during this annealing process in order to allow the various species to move and meet. At this point, several hypotheses can be formulated.

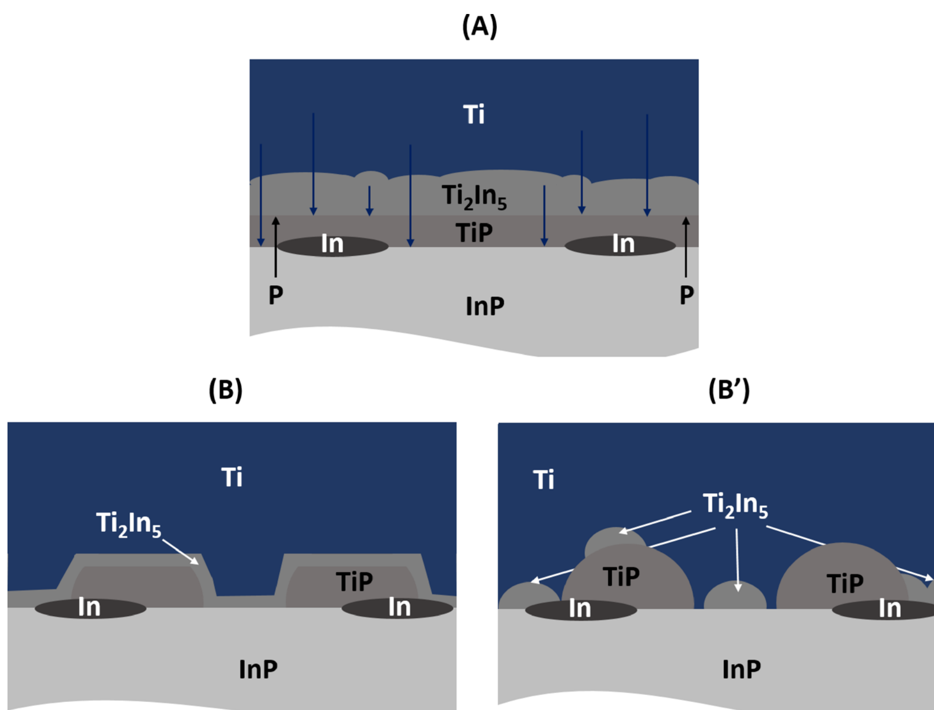

FIG. 10. Schematic representation of the three situations that could enable the species to interact during the annealing treatment conducted at 550 °C with (A) the diffusion of the species through the TiP and Ti_2In_5 layers, (B) the agglomeration of the TiP layer and (B′) the agglomeration of the TiP and Ti_2In_5 layers. Note that these diagrams represent the intermediate states occurring throughout the annealing process.

(i) The increase in temperature might enhance the diffusion of the various elements, therefore, enabling them to diffuse fast enough through the TiP layer [Fig. 10(A)]. This diffusion can occur in the bulk phase, via interstitial and/or substitutional sites or thanks to the grain boundaries. Depending on the diffusion coefficients associated with the Ti and P in this phase, the growth of this phase can occur at the Ti_2In_5/TiP interface, therefore, limiting the length over which the Ti would have to diffuse and/or at the TiP/InP interface, thereby limiting the length over which P would have to diffuse.

(ii) The second hypothesis that can be formulated lies in the assumption that the diffusion of the various species through the TiP layer is still too slow to enable any reaction. The layer(s) must, therefore, become discontinuous at 550 °C in order to allow the Ti and P to interact. This process can be due to an agglomeration of the TiP layer only [Fig. 10(B)] or the agglomeration of both the TiP and Ti_2In_5 layers [Fig. 10(B′)]. In both cases, once the Ti and the InP are in contact, the system tends to minimize its energy. As already mentioned, all the studies present in the literature report the formation of the TiP phase in intact InP surfaces, indicating the fact that this phase is the most stable in InP. As a consequence, because the few In-rich nanometers that were initially present on the InP have been consumed, the formation of the TiP phase is favored and associated with some In release to conserve the overall stoichiometry.

The second hypothesis appears to be the most likely, first, because the mechanisms related to the first one depend on the Ti thickness. The diffusion of the various species should indeed require much more time when 50 nm of Ti were deposited compared to the case were only 20 nm were initially present. Yet, the "Ti-20 nm" and "Ti-50 nm" seem to evolve similarly at 550 °C. As a consequence, the agglomeration of the layer(s) at this temperature is highly probable.

V. CONCLUSION

In conclusion, we demonstrated that the reaction between Ti and the underlying InP substrate is initiated during the deposition process conducted at 100 °C. This reaction gives rise to the simultaneous formation of two binary phases, namely Ti_2In_5 and TiP. While the latter is largely reported in the literature, the first one had never been observed. We attribute the simultaneous formation of both phases to a compositional gradient induced in the InP by the wet surface preparation conducted in a concentrated HCl solution and enhanced by an *in situ* Ar^+ preclean. In accordance with literature, the TiP layers are found to act as a diffusion barrier inhibiting further reaction up to 450 °C in spite of the presence of an important Ti reservoir. In this configuration, all observed phases, i.e., Ti_2In_5, P, TiP, and In, therefore, coexist at temperatures up to 450 °C. Because the promotion of the TiP is thermodynamically more favorable, the Ti_2In_5 tends to be consumed in order to promote the TiP. However, this transition requires the appearance of a diffusion path within the TiP layer that is only be achieved at high temperature, i.e., at 550 °C. The growth of this phase is accompanied by an In release and a total consumption of the Ti_2In_5 and Ti. Therefore, at 550 °C the reaction is enabled either by the enhancement of the species diffusion through the TiP layer or by its agglomeration.

ACKNOWLEDGMENTS

This work was funded, thanks to the French National Research Agency (ANR), under the "Investissements d'avenir" program: IRT Nanoelec' ANR-10-AIRT-05.

APPENDIX A: DESCRIPTION OF THE ANGLES OF A FOUR-CIRCLE DIFFRACTOMETER

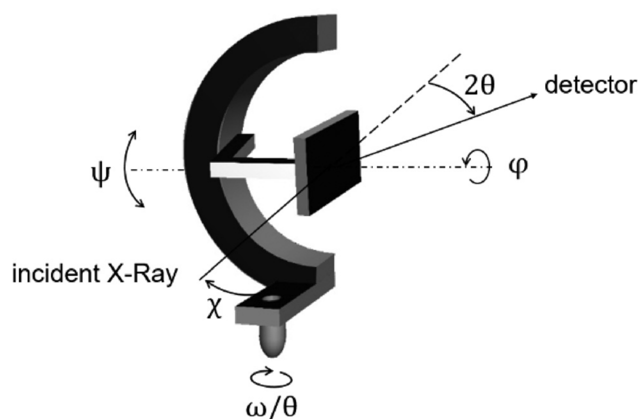

FIG. 11. Schematic representation of a variant of a four-circle diffractometer.

APPENDIX B: INVENTORY OF DIFFRACTION PEAKS USED FOR THE INDEXATION OF XRD PATTERNS

The following tables (Tables I–V) show the list of the Powder Diffraction Files (PDF) from the International Centre for Diffraction Data (ICDD) and the peaks used for the indexation of the XRD patterns shown in this study.

TABLE I. Indexed peaks of InP. InP-ICDD PDF 00-032-0452-Cubic ($F\bar{4}3m$).

2 theta (Cu)	(hkl)	Intensity
26.284	(111)	100
63.358	(400)	10

TABLE II. Indexed peaks of In. In-ICDD PDF 00-005-0642-Tetragonal (I4/mmm).

2 theta (Cu)	(hkl)	Intensity
32.965	(101)	100
36.328	(002)	21
39.170	(110)	36
54.477	(112)	24
56.593	(200)	12
63.204	(103)	16

TABLE III. Indexed peaks of Ti. Ti-ICDD PDF 00-044-1294-Hexagonal ($P6_3/mmc$).

2 theta (Cu)	(hkl)	Intensity
35.094	(100)	25
38.422	(002)	30
40.171	(101)	100
53.005	(102)	13

TABLE IV. Indexed peaks of TiP. TiP-ICDD PDF 04-004-7240-Hexagonal ($P6_3/mmc$).

2 theta (Cu)	(hkl)	Intensity
29.333	(100)	12
30.323	(101)	18
37.398	(103)	100
42.756	(104)	28
48.936	(105)	21
52.022	(110)	44
54.48	(112)	0.3
63.261	(008)	8

TABLE V. Indexed peaks of Ti_2In_5. Ti_2In_5-ICDD PDF 04-007-4080-Tetragonal (P4/mbm).

2 theta (Cu)	(hkl)	Intensity
25.159	(220)	25
28.187	(310)	62
29.78	(001)	73
32.238	(320)	43
34.864	(201)	16
35.879	(400)	16
36.037	(211)	48
37.023	(410)	100
38.138	(330)	33
39.37	(221)	22
41.466	(311)	77
44.457	(321)	44
47.296	(401)	17
48.215	(411)	27
50.892	(421)	16
58.288	(620)	8
59.083	(540)	5
61.854	(002)	13
62.204	(630)	11

[1]A. Katz, B. E. Weir, and W. C. Dautremont-Smith, J. Appl. Phys. **68**, 1123 (1990).

[2]L. Persson, M. El Bouanani, M. Hult, H. J. Whitlow, M. Andersson, I. F. Bubb, P. N. Johnston, S. R. Walker, D. D. Cohen, N. Dytlewski, C. Zaring, and M. Östling, J. Appl. Phys. **80**, 3346 (1996).

[3]M. B. Takeyama, A. Noya, T. Hashizume, and H. Hasegawa, in 10th International Conference on Indium Phosphide and Related Materials (1998), pp. 627–630.

[4]M. B. Takeyama, A. Noya, T. Hashizume, and H. Hasegawa, Jpn. J. Appl. Phys., Part 1 **38**, 1115 (1999).

[5]T. Kendelewicz, P. H. Mahowald, C. E. McCants, K. A. Bartness, I. Lindau, and W. E. Spicer, J. Vac. Sci. Technol., B **5**, 1033 (1987).

[6]T. Chassé, W. G. Wilke, and K. Horn, Surf. Interface Anal. **14**, 315 (1989).

[7]D. Wang and D. G. Ivey, Mater. Sci. Eng., B **41**, 289 (1996).

[8]A. Appelbaum, M. Robbins, and F. Schrey, IEEE Trans. Electron Devices **34**, 1026 (1987).

[9]N. S. Fatemi and V. G. Weizer, J. Appl. Phys. **73**, 289 (1993).

[10]P. S. Mangat, P. Soukiassian, Y. Huttel, Z. Hurych, B. Gruzza, and A. Porte, Appl. Phys. Lett. **63**, 1957 (1993).

[11]M. Ghaffour, A. Abdellaoui, M. Bouslama, A. Ouerdane, and B. Abidri, EPJ Web Conf. **29**, 00020 (2012).

[12]P. Rodriguez, L. Toselli, E. Ghegin, M. Rebaud, N. Rochat, N. Chevalier, E. Martinez, and F. Nemouchi, ECS Trans. **69**, 251 (2015).

[13]E. Ghegin, F. Nemouchi, J. Lábár, C. Perrin, K. Hoummada, S. Favier, S. Gurbán, and I. Sagnes, Microelectron. Eng. **156**, 86 (2016).

[14]D. Cuypers, D. H. van Dorp, M. Tallarida, S. Brizzi, T. Conard, L. N. J. Rodriguez, M. Mees, S. Arnauts, D. Schmeisser, C. Adelmann, and S. De Gendt, ECS J. Solid State Sci. Technol. **3**, N3016 (2014).